Acta Biomaterialia 8 (2012) 570–578

Contents lists available at SciVerse ScienceDirect

Acta Biomaterialia

journal homepage: www.elsevier.com/locate/actabiomat

Fabrication of poly-$_{DL}$-lactide/polyethylene glycol scaffolds using the gas foaming technique

Chengdong Ji, Nasim Annabi, Maryam Hosseinkhani, Sobana Sivaloganathan, Fariba Dehghani *

School of Chemical and Biomolecular Engineering, University of Sydney, Sydney 2006, Australia

ARTICLE INFO

Article history:
Received 28 April 2011
Received in revised form 6 September 2011
Accepted 22 September 2011
Available online 28 September 2011

Keywords:
P_{DL}LA/PEG blend
Three-dimensional scaffold
Porosity
Gas foaming technique

ABSTRACT

The aim of this study was to prepare poly-$_{DL}$-lactide/polyethylene glycol (P_{DL}LA/PEG) blends to improve medium absorption and cell proliferation in the three-dimensional (3-D) structure of their scaffolds. Carbon dioxide (CO_2) was used as a foaming agent to create porosity in these blends. The results of Fourier transform infrared (FTIR) spectroscopy demonstrated that the blends were homogeneous mixtures of P_{DL}LA and PEG. The peak shifts at 1092 and 1744 cm^{-1} confirmed the presence of molecular interactions between these two compounds. Increasing the PEG weight ratio enhanced the relative crystallinity and hydrophilicity. The P_{DL}LA/PEG blends (especially 80/20 and 70/30 weight ratios) exhibited linear degradation profiles over an incubation time of 8 weeks. The mechanical properties of P_{DL}LA/PEG blends having less than 30 wt.% PEG were suitable for the fabrication of porous scaffolds. Increasing the concentration of PEG to above 50% resulted in blends that were brittle and had low mechanical integrity. Highly porous scaffolds with controllable pore size were produced for 30 wt.% PEG samples using the gas foaming technique at temperatures between 25 and 55 °C and pressures between 60 and 160 bar. The average pore diameters achieved by gas foaming process were between 15 and 150 μm, and had an average porosity of 84%. The medium uptake and degradation rate of fabricated P_{DL}LA/PEG scaffolds were increased compared with neat P_{DL}LA film due to the presence of PEG and porosity. The porous scaffolds also demonstrated a lower modulus of elasticity and a higher elongation at break compared to the non-porous film. The fabricated P_{DL}LA/PEG scaffolds have high potential for various tissue-engineering applications.

1. Introduction

Poly-$_{DL}$-lactide (P_{DL}LA) has been widely used for the fabrication of three-dimensional (3-D) scaffolds due to its superior mechanical properties, biocompatibility and biodegradability [1–3]. However, the hydrophobicity of P_{DL}LA results in poor medium uptake and subsequently limited cellular activities [1]. The hydrophobic surface also leads to protein adsorption from the blood when the scaffold is used in vivo, which causes side effects [2]. Blending P_{DL}LA with a polymer such as poly(ethylene glycol) (PEG) may enhance its hydrophilic properties [1,3–10]. P_{DL}LA/PEG blends acquire properties that cannot be found in individual polymers [11,12].

Copolymerization has been used to prepare various P_{DL}LA/PEG blends; the copolymer properties are functions of their compositions and the molecular weights of each monomer [5,13]. Saito et al. [5] produced P_{DL}LA/PEG copolymers for the delivery of bone morphogenetic proteins and the induction of bone formation. The copolymers exhibited a desirable balance between degradation rate and hydrophilicity, and induced the ectopic formation of new bone when evaluated in vivo [5]. An alternative approach is to prepare physical mixtures of these polymers by solvent casting using a solvent that dissolves both polymers [1,9] or emulsion/solvent evaporation using two immiscible solvents, such as water and dichloromethane (DCM) [4].

Porous scaffolds are produced using techniques such as electrospinning [9,14] and freeze drying [1] based on homogeneous blends of two components. Cui et al. [9] used electrospining and prepared a film by processing a mixture of P_{DL}LA and PEG (0–50 wt.% PEG) in acetone/DCM (3/1 by vol.). A homogeneous mixture with pore sizes between 5 and 10 μm was fabricated by this method. The two-dimensional structure of this scaffold and the small pore sizes created by this method were hurdles for applications such as cell proliferation in 3-D structure [9]. Maquet et al. [1] improved the hydrophilicity of P_{DL}LA foams by adding amphiphilic block copolymers of lactide and ethylene oxide (PELA). The porous P_{DL}LA/PELA foams were prepared by freeze drying the solutions in dioxane and chloroform. It was found that the degradation and wettability of the resultant foams were significantly increased when a PELA concentration of 10 wt.% was used. The fabricated blend foams using a 10 wt.% PELA contained both micropores (10 μm) and macropores (100 μm) [1]. The P_{DL}LA/PELA foams

* Corresponding author.
E-mail address: fariba.dehghani@sydney.edu.au (F. Dehghani).

1742-7061/$ - see front matter
doi:10.1016/j.actbio.2011.09.028

fabricated by freeze drying promoted cellular migration, angiogenesis, and axonal growth when implanted in rat spinal cord. However, this technique is energy intensive and there is no control on porous structures. Previous studies demonstrate that the optimal pore size is between 20 and 125 μm for regeneration of adult mammalian skin [15], 20 μm for hepatocytes ingrowth, 40–100 μm for osteoid ingrowth and 100–350 μm for bone regeneration [16]. The development of a process that can tailor pore characteristics is desirable for the fabrication of scaffolds for broad range of biomedical applications.

1.1. Gas foaming

The gas foaming technique utilizes the nucleation and growth of gas bubbles dispersed into a viscous polymer solution for the creation of porosity [17]. The gas bubbles can be formed by a blowing agent via chemical reactions [18]. The foaming agent can also be released from a presaturated gas-polymer mixture [17]. A supercritical fluid, i.e. a fluid above its critical point, can be efficient in forming this gas-saturated polymer phase due to its superior mass transfer properties, zero surface tension and adjustable density by the variation of temperature and pressure [19]. Carbon dioxide is commonly used as a supercritical fluid because of its non-flammability, non-toxicity and moderate critical point (31.1 °C and 73.8 bar). Supercritical CO_2 has been used to generate porosity in amorphous and semi-crystalline polymers such as $P_{DL}LA$, poly(lactic-*co*-glycolic acid), poly(ε-caprolactone) (PCL) and polystyrene [17,20–27]. Subcritical CO_2 (i.e. liquid CO_2 near its critical point) has also been used for the creation of porosity in polymers. For example, Mooney et al. [28] fabricated porous poly($_{D,L}$-lactic-*co*-glycolic acid) scaffolds at 55 bar and temperatures between 20 and 23 °C. However, the use of subcritical CO_2 may require a longer processing time to achieve gas saturation in polymers due to the lower mass transfer properties compared with supercritical conditions [29].

Gas foaming by supercritical or subcritical CO_2 generally involves two stages for the creation of a 3-D porous structure: (i) the formation of a gas-saturated polymer phase (the pressurization stage) and (ii) pore nucleation, growth and coalescence (the depressurization stage) [19,27,30–32]. Exposure of these polymers to high-pressure CO_2 leads to plasticization, and subsequently enhances the CO_2 solubility and diffusivity in these matrices. For example, the glass transition temperature of $P_{DL}LA$ was decreased from 55 to 35 °C when using CO_2 at 68 bar [33]. Upon depressurization and the consequent remarkable drop in CO_2 solubility in the polymers, supersaturation occurs and the nuclei of gas molecules clusters are formed, which then grow and create a porous structure upon vitrification [28,34,35]. The operating variables, such as pressure, temperature and depressurization rate, have significant impacts on the pore characteristics, such as pore size and interconnectivity [21]. Howdle and co-workers [36,37] produced porous $P_{DL}LA$ scaffolds with controllable pore diameter and porosity using high-pressure CO_2. The average pore diameters ranged from 100 to 250 μm, with porosities over 70%.

PEG is able to absorb a large amount of CO_2. Weidner and coworkers [38] measured CO_2 solubility in PEG of different molecular weights (1.5–35 kDa) between 43 and 100 °C and 5 and 300 bar. Their study shows that CO_2 absorption into PEG is enhanced by increasing pressure and decreasing temperature. The maximum CO_2 solubility in the PEG (MW = 4000) was 30 wt.% (CO_2 weight ratio in polymer phase) at 55 °C and 300 bar [38]. It was found that the molecular weight of PEG had a negligible effect on CO_2 solubility in the polymer phase [38,39]. These results endorse the great potential of gas foaming technique using sub- or supercritical CO_2 for the creation of porosity in $P_{DL}LA$/PEG blends.

Gas foaming is a relatively rapid and solvent-free process that can operate at moderate temperatures [17]. The process also enables in situ impregnation of active compounds, such as DNA and bone morphogenic protein-2, within the polymers, and the subsequent release of these compounds upon the diffusion and degradation of polymer [36,37].

The aims of this study were to: (i) prepare blends of $P_{DL}LA$/PEG with optimized properties; and (ii) investigate the feasibility of using the gas foaming process to control pore characteristics of the optimized blends. The effect of PEG weight ratio on the relative crystallinity, hydrophilicity, medium uptake, degradation rate and mechanical strength of blends was first studied. The conditions for the fabrication of porosity in $P_{DL}LA$/PEG by gas foaming were determined. The effect of porosity on the properties of scaffolds was also examined.

2. Materials and methods

2.1. Materials

Poly($_{D,L}$-lactide) ($P_{DL}LA$, 406 kDa) was purchased from PURAC, Singapore. Poly(ethylene glycol) (PEG, 10 kDa) was purchased from Fluka, Australia. Dichloromethane (DCM, 99.5% purity) was purchased from Merck, Australia. Phosphate-buffered saline (PBS, pH 7.2–7.4) was prepared by dissolving a PBS tablet (Sigma, Australia) in MilliQ water (highly purified and deionized water, 18.2 MΩ cm). Food-grade CO_2 (99.99% purity) was supplied by BOC, Australia.

2.2. Preparation of $P_{DL}LA$/PEG blend

Different weight ratios of $P_{DL}LA$ and PEG (50/50, 70/30, 80/20, 90/10 and 100/0) were prepared in Schott bottles by dissolving each mixture in DCM to obtain a 25 wt.% solution (the weight ratio of the total polymer in the DCM). The solution was shaken at 170 rpm for 15 h at ambient temperature using a shaker (ASP Orbital). The homogeneous solution of each blend was poured onto a non-sticky Teflon-coated mould (5×15 cm^2), and kept in a desiccator under a slight vacuum for 2 days to allow DCM evaporation and to produce an opaque blend film.

2.3. The gas foaming process

A schematic diagram of the experimental set-up for the creation of porosity in polymer blends by gas foaming is shown in Fig. 1. Briefly, in each run, about 50 mg of the polymer sample was placed in a high-pressure vessel (40 ml). The vessel was placed in a water bath, the temperature was controlled by a recirculation heater (Ratek TH5-2KW). After thermal equilibrium was attained at a desired temperature (between 25 and 55 °C) and the air had been purged, the system was pressurized with CO_2 to a predetermined pressure (between 60 and 160 bar) using a high-pressure pump (ISCO Syringe pump, Model 500D). The vessel was then isolated, kept under these conditions for 2 h, then depressurized at 10 bar min^{-1}. The depressurization rate was controlled using a capillary tube (10 cm length and 127 μm inner diameter) that was calibrated to the desired rate. After depressurization, the sample was collected for characterizations.

2.4. Characterizations

2.4.1. Attenuated total reflectance–Fourier transform infrared (ATR–FTIR) spectroscopy

The interaction between $P_{DL}LA$ and PEG was determined by ATR–FTIR spectroscopy (Varian 660-IR). Each sample was directly attached and stabilized on the diamond using ATR–FTIR

accessories. The analysis was conducted using 4 cm^{-1} resolutions, averaged for 32 scans over the range 600–2000 cm^{-1}.

2.4.2. Thermal properties

The thermal behaviours of fabricated scaffolds were investigated using differential scanning calorimetry (DSC; TA Instrument Q1000). Briefly, each sample (3–8 mg) was carefully weighed in an aluminium pan and covered with an aluminium lid. The DSC profile of each sample was acquired from a heating run from 30 to 100 °C at a rate of 10 °C min^{-1} under dry nitrogen atmosphere. The relative crystallinity of each sample was defined according to weight fraction of PEG as the ratio of normalized fusion enthalpy to that of pure PEG, which was considered to be 100% crystalline.

2.4.3. Water contact angle

The water contact angle on each film was determined at room temperature. A film was placed on the top of a stainless steel base. A drop of MilliQ water (1 μl) was added to the surface of film, and the image was taken by a built-in CCD camera after an elapsed time of 30 s. The image was analysed by the built-in software of a Rame-hart Instrument to obtain the water contact angle.

2.4.4. Medium uptake

The medium uptake measurements were performed at 37 °C in PBS. Each sample was weighed (W_0) and immersed in PBS overnight (at least 12 h). Each sample was then removed and weighed (W_t) after excessive medium (PBS) was carefully wiped off on the surface of scaffold. The medium uptake ratio was then calculated using the following equation:

$$\text{Media uptake ratio} = \frac{W_t - W_0}{W_0} \quad (1)$$

2.4.5. Degradation rate

The hydrolytic degradation profiles of fabricated scaffolds were evaluated at 37 °C in PBS. Each sample was weighed (W_0) and immersed in PBS. After a predetermined time interval (up to 8 weeks), the sample was rinsed in MilliQ water three times, and weighed (W_t) after drying. The degradation rate was then calculated using the following equation:

$$\text{Degradation rate} = \frac{W_0 - W_t}{W_0} \quad (2)$$

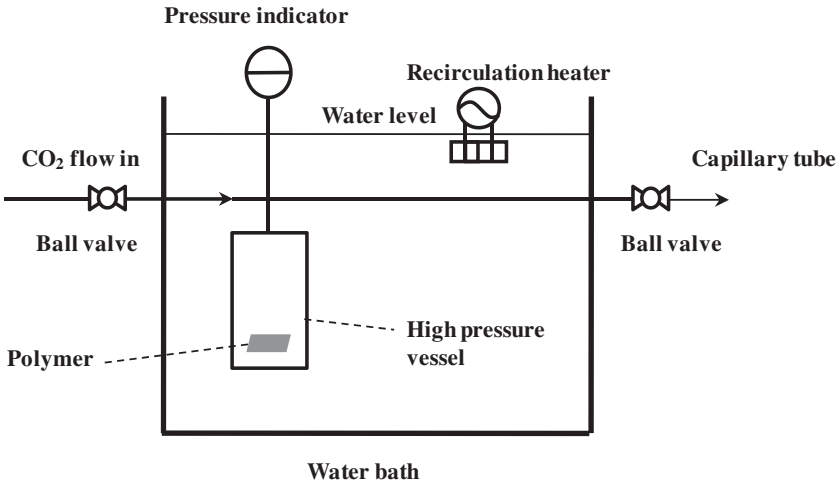

Fig. 1. Schematic diagram of gas foaming process to produce porosity in $P_{DL}LA$/PEG blends.

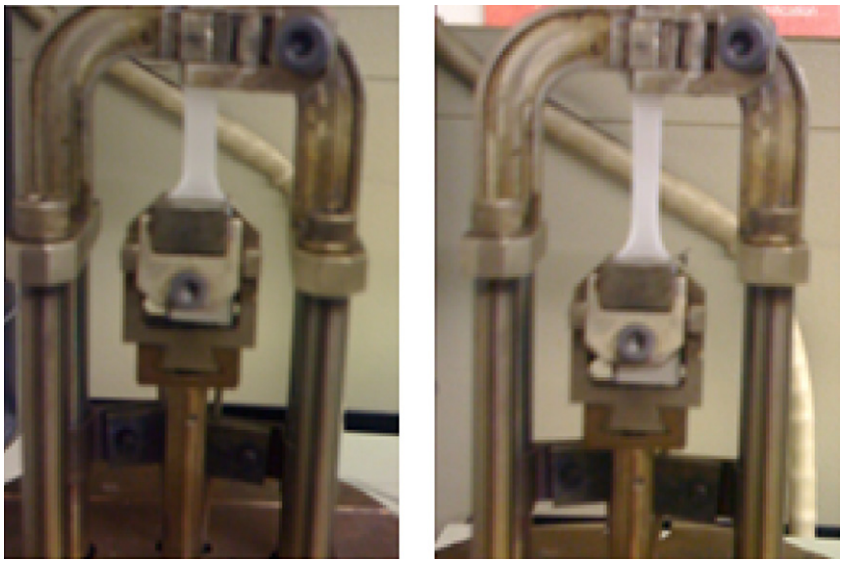

Fig. 2. Images of a dumbell-shape scaffold during DMA measurement. The left panel shows the initial status; the right panel shows the extended status.

2.4.6. Dynamic mechanical analysis (DMA)

The tensile behaviours of fabricated scaffolds were measured using a dynamic mechanical analyser (TA Instrument 2980). Each sample was cut into a dumbbell shape ($10 \times 5 \times 1$, length × width × thickness in mm). The initial and extended statuses of the scaffold during DMA measurement are depicted in Fig. 2. The maximum design force of the equipment is 18 N; the tests were conducted using a force rate of 4 N min^{-1} until sample failure. The tension (mm) and stress (MPa) were recorded by the built-in software, and the tensile modulus of each sample was determined as the slope of the stress–strain curve in the linear region only. The linear regions varied from 5% to 20% for different blends.

2.4.7. Residual solvent

The residue of DCM was measured using gas chromatography (GC; Finnigan Polaris Q). Briefly, each sample was placed in an amber GC vial and heated up to 150 °C; solid-phase microextraction fiber (100 μm, Supelco) was used for the headspace sampling, and helium was the carrier gas. A 40 eV ionization energy was used for this analysis. A calibration curve was obtained prior to the analysis to determine the correlation between the peak area and the various amounts of DCM injected into the GC column. The solvent residue in each sample was calculated using the calibration line.

2.4.8. Scanning electron microscopy (SEM)

The porous structures of fabricated scaffolds were examined using SEM (Philips XL30). Prior to SEM analysis, each sample was frozen and fractured in liquid nitrogen. The cross-section of each scaffold was mounted on a circular aluminium stub and sputter-coated with gold. The equivalent circle diameters of pores ($n \geqslant 300$) were calculated using Image J software. Image J software has been used to calculate the average pore diameter in a number of previous studies [40–44]. The measurements were conducted using at least five SEM images from different cross-sections of each scaffold. The diameters of at least 300 pores were measured for each condition to obtain a reliable data. Our previous results demonstrated that the data obtained by this method are similar to those achieved using microcomputerized tomography (micro CT; Skyscan 1072) [45].

2.4.9. Porosity

The porosity of each processed sample was calculated using the same dimensions as before and after high-pressure processing as described in a previous study [28]. In our study, the scaffolds before and after gas foaming process kept a rectangular shape. Thus, the dimension (length, width and thickness) of each scaffold can be measured accurately using a digital calliper (JBS) ($n = 9$). Due to potential human error in the measurements, we considered $p < 0.01$ to be statistically significant. The volume of scaffold could thus be calculated, and the overall porosity (ε) was then estimated using the following equation:

$$\varepsilon = \frac{V_{\text{pore}}}{V_{\text{processed}}} = \frac{V_{\text{processed}} - V_{\text{original}}}{V_{\text{processed}}} \quad (3)$$

2.5. Statistical analysis

Statistical significance was determined for three replicates (except where otherwise mentioned) by an independent Student's *t*-test for two groups of data or analysis of variance for multiple comparisons using Modde™ 7.0 software (Umetrics). Data are represented as mean ± standard deviation (SD). A confidence level of 95% ($p < 0.05$) was considered as statistically significant except where otherwise mentioned.

3. Results and discussion

3.1. Characterizations of $P_{DL}LA$/PEG film

3.1.1. ATR–FTIR spectroscopy

The presence of each component in the blends was determined using ATR–FTIR spectroscopy. The FTIR spectra of typical absorption peaks and the functional groups present in $P_{DL}LA$ and PEG are shown in Fig. 3. PEG exhibited a characteristic peak at 1092 cm^{-1} (Fig. 3a), corresponding to C–O stretching [46]. The characteristic peak of $P_{DL}LA$ located at 1744 cm^{-1} (Fig. 3c) is attributed to the carbonyl (C═O) band [47,48]. Both peaks were observed in the FTIR spectrum of $P_{DL}LA$/PEG blend, which corroborates the existence of both components in the blend. Peak shifts were found for the ether group from $P_{DL}LA$ (from 1092 to 1084 cm^{-1}) and the carbonyl bond from PEG (from 1744 to 1750 cm^{-1}) (Fig. 3b). These shifts confirmed that there were interactions between $P_{DL}LA$ and PEG, showing that these two components can interact at the molecular level. PEG is miscible with aqueous medium; no significant difference was detected in the FTIR spectrum based on blends before and after the immersion of sample in water for a period of 24 h, indicating that the PEG still remained in the blend after exposure to water.

3.1.2. Thermal properties

$P_{DL}LA$ is amorphous, with a glass transition temperature of 52 °C. The addition of PEG, a crystalline polymer, led to a change in the thermal properties of fabricated scaffold. As shown in Fig. 4, endothermic melting peaks can be seen on $P_{DL}LA$/PEG blends. The weight ratio of PEG had a negligible effect on the melting temperature (~55 °C). Increasing the PEG weight ratio resulted in a greater intensity (peak area) of melting peak. We calculated the relative crystallinity of each blend according to pure PEG. As expected, by increasing the weight ratio of PEG from 10 to 50 wt.%, the relative crystallinity was enhanced (from 16% to 75%; Table 1).

3.1.3. Hydrophilicity

It is desirable to enhance the hydrophilic properties of a polymer to promote cell adhesion and proliferation in scaffolds. The use of $P_{DL}LA$ in tissue engineering is usually limited by its hydrophobicity [2]. $P_{DL}LA$ can adsorb protein from the blood on its hydrophobic surface, which subsequently causes undesirable side effects, such as thrombus formation [49,50]. Blending $P_{DL}LA$ with a polymer such as PEG may improve its hydrophilic properties,

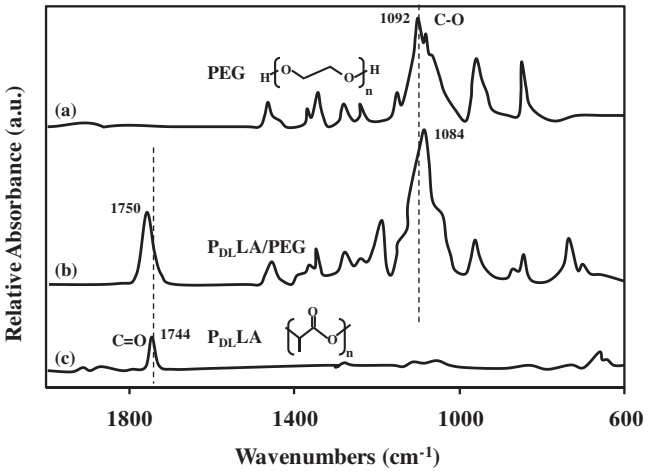

Fig. 3. FTIR spectra of (a) PEG, (b) $P_{DL}LA$/PEG (70/30 blend) and (c) $P_{DL}LA$.

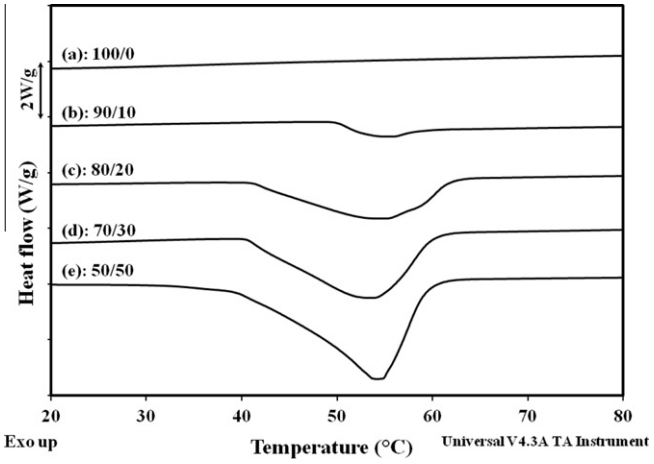

Fig. 4. DSC profiles of (a) pure $P_{DL}LA$ and (b–e) $P_{DL}LA$/PEG blends at various weight ratios.

Table 1
Relative crystallinity and hydrophilicity (water contact angles and swelling ratios) of $P_{DL}LA$/PEG blends at different weight ratios.

Weight ratio of $P_{DL}LA$/PEG blend	Relative crystallinity (%)	Water contact angle (°)	Swelling ratio (%)
100/0	–	159.6 ± 2	–
90/10	15.8	97.8 ± 3	11.4 ± 0.4
80/20	72.3	70.5 ± 0.2	30.2 ± 1.6
70/30	74.8	51.9 ± 3	35.6 ± 0.9
50/50	76.2	53.5 ± 0.2	37.0 ± 2.2
0/100	100	22.8 ± 2	–

–: not determined.

thereby minimizing protein adsorption [2,51]. The water contact angle of the hydrophilic PEG film was 22.8 ± 2° and that of pure $P_{DL}LA$ film was 159.6 ± 2°, corroborating its hydrophobicity [52]. The water contact angle of 50/50 $P_{DL}LA$/PEG blend was decreased compared to neat $P_{DL}LA$, to 53.5 ± 0.2° (Table 1). The decrease in water contact angle by increasing PEG weight ratio demonstrates that the hydrophilicity of $P_{DL}LA$ was improved due to the addition of PEG.

The medium uptake property of scaffolds facilitates cellular nutrient supply and waste removal [53]. The medium uptake for neat $P_{DL}LA$ film was negligible; however, blending this polymer with PEG enhances its capacity for medium uptake. The medium (PBS) uptake ratio of blends ranged from 11.4 ± 0.4 to 37.0 ± 2 as the weight ratio of PEG was increased from 10 to 50 wt.% (Table 1). Maquet et al. [1] found a similar trend in freeze-dried $P_{DL}LA$/PEG blend scaffolds; the increased PEG weight ratio resulted in improved medium absorption capacity.

3.1.4. Degradation rate

$P_{DL}LA$/PEG blends degrade due to hydrolysis of $P_{DL}LA$ and dissolution of PEG in aqueous medium. As shown in Fig. 5, pure $P_{DL}LA$ exhibited a slow degradation ratio (7.2 ± 0.5%) within 4 weeks, while a dramatic increase was observed from week 6. Neat $P_{DL}LA$ was degraded 58.4 ± 3% after week 8. The blends with 10 wt.% PEG (90/10 blend) showed a similar degradation pattern to pure $P_{DL}LA$. The other blends (80/20, 70/30 and 50/50) exhibited different degradation profiles compared to pure $P_{DL}LA$ film: a greater weight loss ratio (12.8 ± 0.1–31.5 ± 0.1%) occurred during the first week due to the partial dissolution of PEG, after which a linear degradation rate was observed up to 8 weeks. The addition of PEG (10–30 wt.%) reduced the degradation rate of $P_{DL}LA$; this may be due to

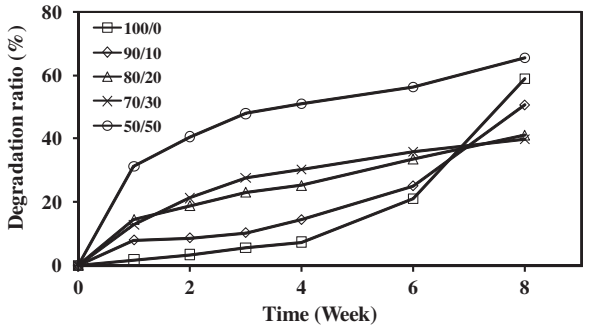

Fig. 5. Degradation profiles of $P_{DL}LA$/PEG blends at different weight ratios.

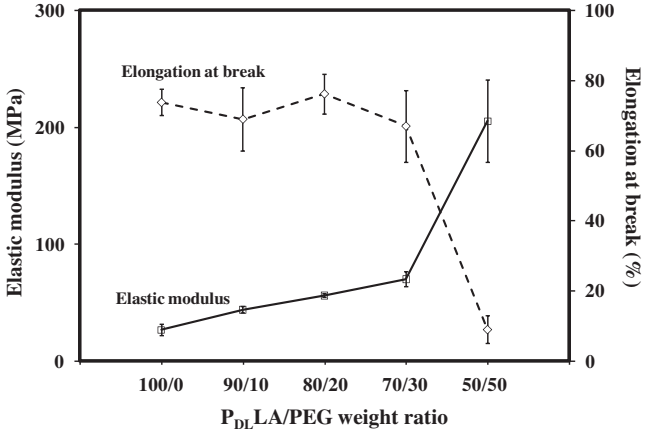

Fig. 6. Tensile behaviours of $P_{DL}LA$/PEG blends at different weight ratios. The elastic modulus (MPa) corresponds to the primary axis (left) and the elongation at break (%) corresponds to the secondary axis (right).

the molecular interaction between these two components, as previously indicated. A short-term (3 h) degradation test was conducted for $P_{DL}LA$ films and $P_{DL}LA$/PEG (50/50) blends. The results showed that after 3 h the $P_{DL}LA$ films had negligible weight loss, whereas a weight loss of at least 5 wt.% was observed for the $P_{DL}LA$/PEG. This confirms that PEG dissolution occurred at the early stage of immersion in a medium.

3.1.5. Mechanical strength

Pure $P_{DL}LA$ film is hard and tough, with a low elastic modulus (26.7 ± 5 MPa) but a high elongation at break (73.7 ± 4%). The addition of PEG resulted in an enhanced elastic modulus, as shown in Fig. 6. The elastic modulus was increased to 70.0 ± 7 MPa when the PEG weight ratio was raised to 30%. This phenomenon may be attributed to the increased crystallinity [54]. We found a dramatic enhancement in the elastic modulus (205.2 ± 35 MPa) when 50 wt.% PEG was used. However, the elongation of break dropped greatly (8.9 ± 4%), indicating that the 50/50 blend was more brittle. No significant effect on elongation of break was observed when the PEG weight ratio was below 30%.

3.1.6. Solvent residue

The DCM residues in the films were less than 10 ppm (mg DCM per kg film), which is below the United States Pharmacopeia (USP) and the United States Food and Drug Administration acceptance levels (600 and 150 ppm, respectively) [55,56]. These data demonstrate that the drying procedure was efficient at removing the organic solvent residue and that the fabricated 3-D porous scaffold

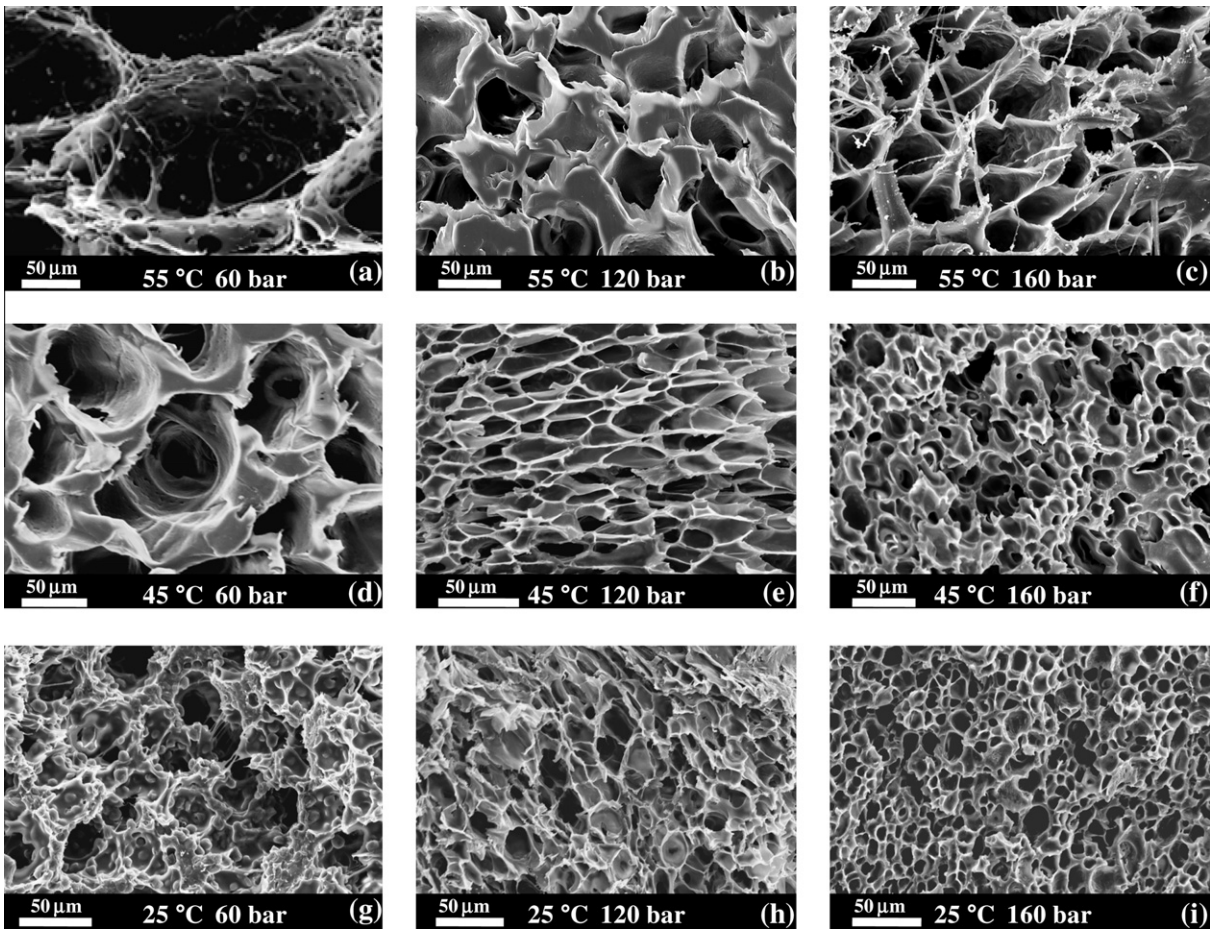

Fig. 7. SEM images of cross-sections of $P_{DL}LA$/PEG (70/30) blends produced by gas foaming at different temperatures and pressures.

Table 2
Pore sizes produced in $P_{DL}LA$/PEG (70/30) blends at different operating conditions.

Pressure (bar)	Temperature (°C)	Pore size (μm)
60	25	55.8 ± 7
	45	80.7 ± 9
	55	150.2 ± 34
120	25	26.1 ± 6
	45	34.0 ± 8
	55	63.5 ± 14
160	25	15.5 ± 5
	45	21.8 ± 5
	55	48.0 ± 11

had no residue, which would limit its application for tissue engineering.

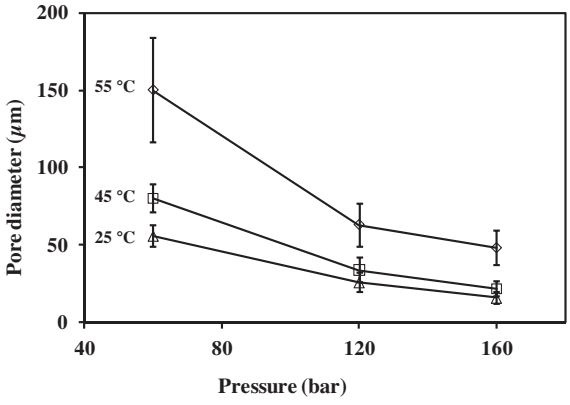

Fig. 8. Pore diameters of $P_{DL}LA$/PEG (70/30) blends produced by gas foaming at various temperatures and pressures.

3.2. Fabrication of porous $P_{DL}LA$/PEG 3-D scaffolds

$P_{DL}LA$/PEG blends characterizations demonstrate that the 70/30 weight ratio of $P_{DL}LA$/PEG exhibited optimum properties, such as mechanical strength, medium uptake, degradation rate and hydrophilicity. A porous $P_{DL}LA$/PEG scaffold was thus prepared based on this weight ratio using the gas foaming technique. Previous studies demonstrate the plasticization (reduction of glass transition temperature) of $P_{DL}LA$ [33] and melting point depression of PEG occurs when using CO_2 at pressures above 60 bar [57,58] due to the interactions between these polymers and CO_2. Hence, the effect of pressure on pore characteristics was determined at pressures above 60 bar. The blends exhibited a melting temperature of 55 °C; therefore, the operating temperature was selected between the ambient temperature of 25 °C and below the melting point of blend to avoid melting and to maintain the shape of scaffold during the gas foaming process.

Highly porous scaffolds were produced by gas foaming using supercritical and subcritical CO_2, respectively (Fig. 7). The pore size ranged from 15.5 ± 2 to 150.2 ± 34 μm, as shown in Table 2. The effect of operating conditions (pressure and temperature) on the

pore size was investigated. As shown in Fig. 8, at subcritical temperature (25 °C), the average pore diameter in $P_{DL}LA$/PEG was slightly smaller than the ones created under supercritical conditions and the effect of pressure was less pronounced at this temperature. At a subcritical pressure (60 bar), the pore size was larger than the one formed under supercritical conditions. The pores were also less uniform at subcritical conditions, which might be due to the lower diffusivity of CO_2 into the polymer under these conditions: the processing time might not be adequate for uniform distribution of CO_2 into the polymer phase.

At a constant temperature, increasing pressure resulted in decreasing pore size (Fig. 8). This is in agreement with previous studies [21,59,60]. The pore diameter of polystyrene scaffold decreased from 70 to 10 μm as the pressure was increased from 137 to 413 bar at 100 °C [59]. Higher pressure results in increased solubility of CO_2 within the polymer, which causes greater supersaturation upon depressurization and subsequently higher gas nucleation densities, thus smaller pores are created [21,59].

At a constant pressure, elevating the temperature of gas foaming process increased the pore diameter (Fig. 8). Arora et al. [59] observed similar behaviour when processing polystyrene with gas foaming; the pore diameter was enhanced from 7 to 25 μm as temperature was elevated from 60 to 120 °C. Increasing temperature leads to decreasing CO_2 density, thus reducing its solubility in the polymer. However, raising the temperature enhances the CO_2 diffusion and reduces the viscosity of polymer; both factors are expected to increase the CO_2 absorption and mobility into the polymer phase in a certain period of time. The results acquired for the effect of temperature show that density is the dominant factor affecting the pore size for these systems [21,59]. At higher temperatures the degree of supersaturation is reduced during the depressurization stage as a result of decreasing CO_2 solubility in the polymer phase. Subsequently, lower numbers of gas nuclei are formed in the polymer, which then grow due to the greater CO_2 mobility and create larger pores.

The overall porosity of fabricated sample in this study at different conditions was in average 84%. However, the difference between porosity of samples produced at different conditions was negligible. The porosity of sample prepared at 45 °C and 120 bar was also measured by the microCT technique using built-in software (CT-An) based on a series of 3-D reconstructed images (n = 150) (Fig. 9). The result (79%) was comparable with the porosity calculated by measuring the dimension change based on the samples produced at the same condition (74–77%).

The formation of a skin layer on the surface of scaffolds is a common problem in many processes used for the creation of porosity in polymers [61]. We observed the formation of a skin layer (Fig. 9) in the gas foaming process. The skin layer is formed due to rapid diffusion of CO_2 near the surface, where the CO_2 concentration is too low to create nucleation [61,62]. This layer can simply be cut off to improve the mass transfer of nutrients and oxygen transfer, and to promote cell infiltration in the 3-D structure.

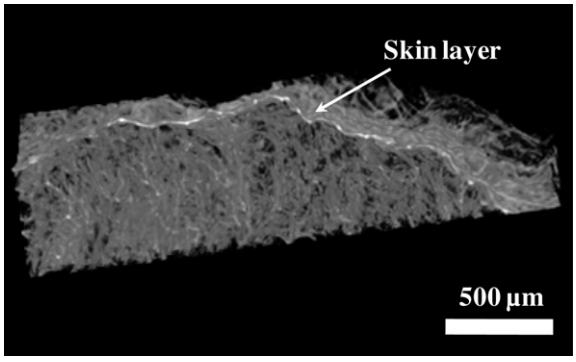

Fig. 9. 3-D image of porous $P_{DL}LA$/PEG (70/30) produced by gas foaming under 45 °C and 120 bar.

3.3. The effect of porosity on scaffold properties

The porous structure is expected to provide a larger contact surface area between the medium and the scaffold, thereby improving the medium uptake property. The non-porous $P_{DL}LA$/PEG film exhibited a medium uptake of 35.6 ± 1%. The medium uptake of the porous scaffolds (produced at 120 bar and 45 °C) was increased twofold (73.0 ± 6%).

The hydrolysis of porous scaffolds is accelerated due to the increased contact surface area between the material and the medium. As shown in Fig. 10, porous scaffold exhibited a faster degradation profile. The ultimate degradation ratio after week 8 for the porous scaffold produced at 120 bar and 45 °C was 70.9 ± 1%, compared with the non-porous scaffold, which showed 41.8 ± 2% degradation.

The pore size plays a significant role in regulating the mechanical behaviour of a scaffold [63]; the porous structure usually makes the scaffold less elastic [64–69]. As shown in Fig. 11, the porous scaffolds fabricated at 120 bar and 45 °C exhibited a lower elastic modulus than the non-porous film (21.5 ± 2 vs. 70.0 ± 7 MPa). Yu et al. [70] found similar observations on PCL/hydroxyapatite composite scaffolds. The elastic modulus of their non-porous scaffolds was 130 MPa on average, while their porous scaffold (75% porosity) exhibited a greatly declined elastic modulus (5 MPa). A remarkable increase in elongation at break was detected

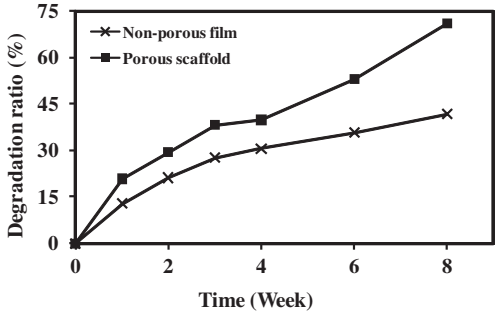

Fig. 10. Degradation profiles of non-porous and porous $P_{DL}LA$/PEG (70/30) blends. The porous scaffolds were processed under 45 °C and 120 bar.

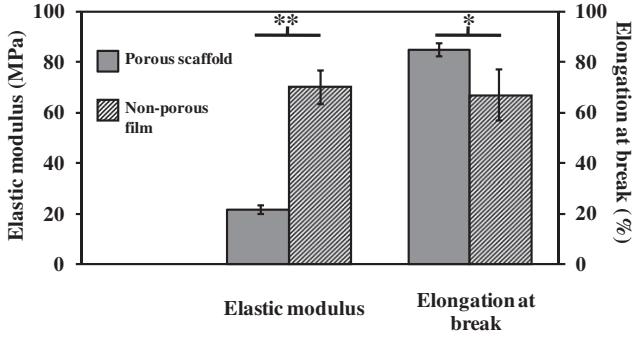

Fig. 11. Mechanical behaviours of non-porous and porous $P_{DL}LA$/PEG (70/30) blends. The porous scaffold was processed by gas foaming at 45 °C and 120 bar. The elastic modulus (MPa) corresponds to the primary axis (left); the elongation at break (%) corresponds to the secondary axis (right). Student's t-tests were performed for porous scaffolds compared with non-porous film: $^{*}p < 0.05$, $^{**}p < 0.0005$.

in the porous scaffold over the non-porous samples (84.8 ± 3% compared with 66.9 ± 10%). These data confirm that porosity had a positive impact on extensibility. Madihally and Matthew [65] demonstrated that porous chitosan scaffolds exhibit higher elongation at break (~110%) than non-porous equivalents (30–40%). Porous scaffolds can be potentially applied in various tissue engineering applications due to their reasonable elastic modulus and elongation rate [71].

4. Conclusions

$P_{DL}LA$ and PEG were blended stably by solvent casting due to their molecular interactions. The characteristics of blend can be tailored using different weight ratios of two components. $P_{DL}LA$/PEG with a weight ratio of 70/30 exhibited the optimum properties. The gas foaming technique using supercritical and subcritical CO_2 was efficient in creating porosity in the blends and eliminated the use of an organic solvent. This process allows the production of 3-D porous scaffolds and tailoring of the pore size by adjusting the variables of the process. The average pore diameters ranged from 15 to 150 μm. Large size pores were produced at subcritical conditions. The pore size had a significant impact on the medium uptake, degradation and mechanical properties of polymer. The pore size of scaffolds can be tailored to suit various tissue engineering applications.

Acknowledgments

The authors acknowledge the financial support of the Australian Research Council. The authors also acknowledge the kind help and discussion from Dr. Keith Fisher for the GC measurements, Mr. Trevor Shearing for the DMA measurements, and Ms. Elizabeth Dobrinsky the laboratory manager.

Appendix A. Figures with essential colour discrimination

Certain figures in this article, particularly Figure 2 is difficult to interpret in black and white. The full colour images can be found in the on-line version, at doi:10.1016/j.actbio.2011.09.028.

References

[1] Maquet V, Matrtin D, Scholtes F, Franzen R, Schoenen J, Moonen G, et al. Poly ($_{D,\ L}$-lactide) foams modified by poly(ethylene oxide)-block-poly($_{D,\ L}$-lactide) copolymers and a-FGF: in vitro and in vivo evaluation for spinal cord regeneration. Biomaterials 2001;22:1137–46.
[2] Chen C, Chueh J, Tseng H, Huang H, Lee S. Preparation and characterization of biodegradable PLA polymeric blends. Biomaterials 2003;24:1163–73.
[3] Cheung H, Lau KL, Lu TP, Hui D. A critical review on polymer-based bio-engineered materials for scaffold development. Composites B 2007;38:291–300.
[4] Yang Y, Chung T, Bai X, Chan W. Effect of preparation conditions on morphology and release profiles of biodegradable polymeric microspheres containing protein fabricated by double-emulsion method. Chem Eng Sci 2000;55:2223–36.
[5] Saito N, Okada T, Horiuchi H, Murakami N, Takahashi J, Nawata M, et al. A biodegradable polymer as a cytokine delivery system for inducing bone formation. Nat Biotechnol 2001;19:332–5.
[6] Yamamoto Y, Yasugi K, Harada A, Nagasaki Y, Kataoka K. Temperature-related change in the properties relevant to drug delivery of poly(ethylene glycol)–poly($_{D,\ L}$-lactide) block copolymer micelles in aqueous milieu. J Control Release 2002;82:359–71.
[7] Kim K, Yu M, Zong X, Chiu J, Fang D, Seo YS, et al. Control of degradation rate and hydrophilicity in electrospun non-woven poly ($_{D,\ L}$-lactide) nanofiber scaffolds for biomedical appliactions. Biomaterials 2003;24:4977–85.
[8] Jule E, Yamamoto Y, Thouvenin M, Nagasaki Y, Kataoka K. Thermal characterization of poly(ethylene glycol)–poly($_{D,\ L}$-lactide) block copolymer micelles based on pyrene excimer formation. J Control Release 2004;97:407–19.
[9] Cui W, Zhu X, Yang Y, Li X, Jin Y. Evaluation of electrospun fibrous scaffolds of poly ($_{DL}$-lactide) and poly (ethylene glycol) for skin tissue engineering. Mater Sci Eng C Mater Biol Appl 2009;29:1869–76.
[10] Dai Y, Niu J, Liu J, Yin L, Xu J. In situ encapsulation of laccase in microfibers by emulsion electrospinning: preparation, characterization, and application. Bioresour Technol 2010;101:8942–7.
[11] Sarasam A, Madihally SV. Characterization of chitosan–polycaprolactone blends for tissue engineering applications. Biomaterials 2005;26:5500–8.
[12] Zhong X, Ji C, Chan AKL, Kazarian SG, Ruys AJ, Dehghani F. Fabrication of chitosan/poly(ε-caprolactone) composite hydrogels for tissue engineering applications. J Mater Sci Mater Med 2011;22:279–88.
[13] Celikkaya E, Denkbas EB, Piskin E. Poly($_{DL}$-ladide)/poly(ethylene glycol) copolymer particles.I. Preparation and characterization. J Appl Polym Sci 1996;61:1439–46.
[14] Peng H, Zhou S, Guo T, Li Y, Li X, Wang J, et al. In vitro degradation and release profiles for electrospun polymeric fibers containing paracetanol. Colloids Surf B 2008;66:206–12.
[15] Yannas IV, Lee E, Orgill DP, Skrabut EM, Murphy GF. Synthesis and characterization of a model extracellular matrix that induces partial regeneration of adult mammalian skin. Proc Natl Acad Sci USA 1989;86:933–7.
[16] Whang K, Healy KE, Elenz DR, Nam EK, Tsai DC, Thomas CH, et al. Tissue Eng 1999;5:35.
[17] Annabi N, Nichol JW, Zhong X, Ji C, Koshy S, Khademhosseini A, et al. Controlling the porosity and microarchitecture of hydrogels for tissue engineering. Tissue Eng Part B Rev 2010;16:371–83.
[18] Caykara T, Kucuktepe S, Turan E. Swelling characteristics of thermo-sensitive poly[(2-diethylaminoethyl methacrylate)-co-(N, N-dimethylacrylamide)] porous hydrogels. Polym Int 2007;56:532–7.
[19] Tomasko DL, Guo Z. Supercritical Fluids. In: Kirk-Othmer Encyclopedia of Chemical Technology. New York: John Wiley & Sons; 2006.
[20] Barry JJA, Silva MMCG, Popov VK, Shakesheff KM, Howdle SM. Supercritical carbon dioxide: putting the fizz into biomaterials. Philos Trans R Soc Lond A 2006;364:249–61.
[21] Tai H, Mather ML, Howard D, Wang W, White LJ, Crowe JA, et al. Control of pore size and structure of tissue engineering scaffolds produced by supercritical fluid processing. Eur Cells Mater 2007;14:64–77.
[22] Xu Z, Jiang X, Liu T, Hu G, Zhao L, Zhu Z, et al. Foaming of polypropylene with supercritical carbon dioxide. J Supercrit Fluids 2007;41:299–310.
[23] Nalawade SP, Picchioni F, Marsman JH, Grijpma DW, Feijen J, Janssen LPBM. Intermolecular interactions between carbon dioxide and the carbonyl groups of polylactides and poly(ε-caprolactone). J Control Release 2006;116:e38–40.
[24] Kazarian SG. Polymer processing with supercritical fluids. Polym Sci Ser C 2000;42:78–101.
[25] Nalawade SP, Picchioni F, Janssen LPBM. Supercritical carbon dioxide as a green solvent for processing polymer melts: processing aspects and applications. Prog Polym Sci 2006;31:19–43.
[26] Annabi N, Fathi A, Mithieux SM, Weiss AS, Dehghani F. Fabrication of porous PCL/elastin composite scaffolds for tissue engineering applications. J Supercrit Fluids 2011;59:157–67.
[27] Harris LD, Kim B-S, Mooney DJ. Open pore biodegradable matrixes formed with gas foaming. J Biomed Mater Res 1998;42:396–402.
[28] Mooney DJ, Baldwin DF, Suh NP, Vacanti JP, Langer R. Novel approach to fabricate porous sponges of poly($_{D,\ L}$-lactic-co-glycolic acid) without the use of organic solvents. Biomaterials 1996;17:1417–22.
[29] Quirk RA, France RM, Shakesheff KM, Howdle SM. Supercritical fluid technologies and tissue engineering scaffolds. Curr Opin Solid State Mater Sci 2005;8:313–21.
[30] Hile DD, Amirpour ML, Akgerman A, Pishko MV. Active growth factor delivery from poly($_{D,\ L}$-lactide-co-glycolide) foams prepared in supercritical CO_2. J Control Release 2000;66:177–85.
[31] Lopez-Periago AM, Vega A, Subra P, Argemi A, Saurina J, Garcia-Gonzalez CA, et al. Supercritical CO_2 processing of polymers for the production of materials with applications in tissue engineering and drug delivery. J Mater Sci 2008;43:1939–47.
[32] Gualandi C, White LJ, Chen L, Gross RA, Shakesheff KM, Howdle SM, et al. Scaffold for tissue engineering fabricated by non-isothermal supercritical carbon dioxide foaming of a highly crystalline polyester. Acta Biomater 2010;6:130–6.
[33] Hao J, Whitaker MJ, Wong B, Serhatkulu G, Shakesheff KM, Howdle SM. Plasticization and spraying of poly ($_{DL}$-lactic acid) using supercritical carbon dioxide: control of particle size. J Pharm Sci 2004;93:1083–90.
[34] Cooper AI. Polymer synthesis and processing using supercritical carbon dioxide. J Mater Chem 2000;10:207–34.
[35] Goel SK, Beckman EJ. Generation of microcellular polymeric foams using supercritical carbon dioxide I. Effect of pressure and temperature on nucleation. Polym Eng Sci 1994;34:1137–47.
[36] Kanczler JM, Ginty PJ, White L, Clarke N, Howdle SM, Shakesheff KM, et al. The effect of the delivery of vascular endothelial growth factor and bone morphogenic protein-2 to osteoprogenitor cell populations on bone formation. Biomaterials 2010;31:1242–50.
[37] Heyde M, Partridge K, Howdle SM, Oreffo ROC, Garnett M, Shakesheff KM. Development of a slow non-viral DNA release system from $P_{DL}LA$ scaffolds fabriacted using a supercritical CO_2 technique. Biotechnol Bioeng 2007;98:679–93.
[38] Weidner E, Wiesmet V, Knez Z, Skerget M. Phase equilibrium (solid–liquid–gas) in polyethyleneglycol–carbon dioxide systems. J Supercrit Fluids 1997;10:139–47.
[39] Wiesmet V, Weidner E, Behme S, Sadowski G, Arlt W. Measurement and modeling of high-pressure phase equilibria in the systems polyethyleneglycol

(PEG)–propane, PEG–nitrogen and PEG–carbon dioxide. J Supercrit Fluids 2000;17:1–12.
[40] Savina IN, Gun'ko VM, Turov VV, Dainiak M, Phillips GJ, Galaev IY, et al. Soft Matter 2011;7:4276.
[41] Kim U-J, Park J, Kim HJ, Wada M, Kaplan DL. Three-dimensional aqueous-derived biomaterial scaffolds from silk fibroin. Biomaterials 2005;26:2775–85.
[42] Aronin CEP, Sadik KW, Lay AL, Rion DB, Tholpady SS, Ogle RC, et al. Comparative effects of scaffold pore size, pore volume, and total void volume on cranial bone healing patterns using microsphere-based scaffolds. J Biomed Mater Res 2009;89A:632–41.
[43] Annabi N, Fathi A, Mithieux SM, Martens P, Weiss AS, Dehghani F. The effect of elastin on chondrocyte adhesion and proliferation on poly (ε-caprolactone)/elastin composites. Biomaterials 2011;32:1517–25.
[44] Autissier A, Le Visage C, Pouzet C, Chaubet F, Letourneur D. Fabrication of porous polysaccharide-based scaffolds using a combined freeze-drying/cross-linking process. Acta Biomater 2010;6:3640–8.
[45] Annabi N, Mithieux SM, Weiss AS, Dehghani F. The fabrication of elastin-based hydrogels using high pressure CO_2. Biomaterials 2009;30:1–8.
[46] Mansur HS, Orefice RL, Mansur AAP. Characterization of poly(vinyl alcohol)/poly(ethylene glycol) hydrogels and PVA-derived hybrids by small-angle X-ray scattering and FTIR spectroscopy. Polymer 2004;45:7193–202.
[47] Kazarian SG, Chan AKL, Veronique M, Boccaccini AR. Characterisation of bioactive and resorbable polylactide/Bioglass compoistes by FTIR spectroscopic imaging. Biomaterials 2004;25:3931–8.
[48] Zheng X, Zhou S, Xiao Y, Yu X, Li X, Wu P. Shape memory effect of poly (D, L-lactide)/Fe3O4 nanocomposites by inductive heating of magnetite particles. Colloids Surf B 2009;71:67–72.
[49] Knetsch M, Aldenhoff Y, Hanssen H, Koole L. A novel synthetic vascular prosthesis: effect of plasma protein adsorption on blood- and cyto-compatibility. Mat-wissu Werkstofftech 2006;37:6.
[50] Kim SW, Lee RG. Adsorption of blood proteins onto polymer surfaces. In: Baier RE, editor. Applied Chemistry at Protein Interfaces. Washington, DC: American Chemical Society; 1975.
[51] Amiji MM, Park K. Analysis on the surface adsorption of PEO/PPO/PEO triblock copolymersby radiolabelling and fluorescence techniques. J Appl Polym Sci 1994;52:539–44.
[52] Forch R, Schonherr H, Jenkins ATA. Surface design: applications in bioscience and nanotechnology. WEinheim: Wiley-VCH; 2009. p. 471.
[53] Hoffman AS. Hydrogels for biomedical applications. Ann NY Acad Sci 2001;944:62–73.
[54] Carraher CE, Seymour RB. Seymour/Carraher's Polymer Chemistry. Boca Raton, FL: CRC Press; 2003.
[55] Report on Carcinogens. 11th ed. U.S. Department of Health and Human Services, Public Health Service, National Toxicology Program; 2005.
[56] The United States Pharmacopeia – National Formulary (USP 30 –NF 25) 2007 [chapter 467].
[57] Nalawade SP, Picchioni F, Marsman JH, Janssen LPBM. The FT-IR studies of the interactions of CO_2 and polymers having different chain groups. J Supercrit Fluids 2006;36:236–44.
[58] Pasquali I, Comi L, Pucciarelli F, Bettini R. Swelling, melting point reduction and solubility of PEG 1500 in supercritical CO_2. Int J Pharm 2008;356:76.
[59] Arora KA, Lesser AJ, McCarthy TJ. Preparation and characterization of microcellular polystyrene foams processed in supercritical carbon dioxide. Macromolecules 1998;31:4614–20.
[60] Nalawade SP, Westerman D, Leeke G, Santos RCD, Grijpma DW, Feijen J. Preparation of porous poly(trimethylene carbonate) structures for controlled release applications using high pressure CO_2. J Control Release 2008;132:e73–5.
[61] Morisaki M, Ito T, Hayvali M, Tabata I, Hisada K, Hori T. Preparation of skinless polymer foam with supercritical carbon dioxide and its application to a photoinduced hydrogen evolution system. Polymer 2008;49:1611–9.
[62] Goel SK, Beckman EJ. Generation of microcellular polymeric foams using supercritical carbon dioxide II. Cell growth and skin formation. Polym Eng Sci 1994;34:1148–56.
[63] Karageorgiou V, Kaplan D. Porosity of 3D biomaterial scaffolds and osteogenesis. Biomaterials 2005;26:5474–91.
[64] Story B, Wagner WR, Gaisser D, Cook S, Rust-Dawicki A. In vivo performance of a modified CSTi dental implant coating. Int J Oral Maxillofac Implants 1998;13:749–57.
[65] Madihally SV, Matthew HWT. Porous chitosan scaffolds for tissue engineering. Biomaterials 1999;20:1133–42.
[66] Porter B, Oldham J, He S, Zobitz M, Payne R, An K, et al. Mechanical properties of a biodegradable bone regeneration scaffold. J Biomech Eng 2000;122:286–8.
[67] Hollister SJ. Porous scaffold design for tissue engineering. Nat Mater 2006;5:590.
[68] Almeida HA, Bartolo PJ, Ferreira JC. Mechanical behaviour and vascularisation analysis of tissue engineering scaffolds. In: Bartolo PJ, editor. Virtual and Rapid Manufacturing: Adavanced Research in Virtual and Rapid Prototyping. London: Taylor & Francis Group; 2008.
[69] Ji C, Annabi N, Khademhosseini A, Dehghani F. Fabrication of porous chitosan scaffolds for soft tissue engineering using dense gas CO_2. Acta Biomater 2011;7:1653–64.
[70] Yu H, Matthew H, Wooley PH, Yang S. Effect of porosity and pore size on microstructures and mechanical properties of poly-ε-caprolactone-hydroxyapatite composites. J Biomed Mater Res B Appl Biomater 2008;86B:541–7.
[71] Palsson BQ, Bhatia SN. Tissue Engineering. San Diego, CA: Pearson Prentice Hall; 2004.